

Article

# Molecular Specific and Sensitive Detection of Pyrazinamide and Its Metabolite Pyrazinoic Acid by Means of Surface Enhanced Raman Spectroscopy Employing In Situ Prepared Colloids

Anna Muehlig<sup>1,2,3,†</sup>, Izabella J. Jahn<sup>1,2,3,†</sup>, Jan Heidler<sup>1</sup>, Martin Jahn<sup>1,‡</sup>, Karina Weber<sup>1,2,3</sup>, Patricia Sheen<sup>4</sup>, Mirko Zimic<sup>4</sup>, Dana Cialla-May<sup>1,2,3,\*</sup> and Juergen Popp<sup>1,2,3</sup> 

<sup>1</sup> Leibniz Institute of Photonic Technology (IPHT)—Member of the Research Alliance “Leibniz Health Technologies”, Albert-Einstein-Straße 9, 07745 Jena, Germany; anna.muehlig@leibniz-ipht.de (A.M.); Izabella.jahn@leibniz-ipht.de (I.J.J.); j.heidler@gmx.de (J.H.); mjahn@cismst.de (M.J.); karina.weber@leibniz-ipht.de (K.W.); juergen.popp@leibniz-ipht.de (J.P.)

<sup>2</sup> Friedrich-Schiller-University Jena, Institute of Physical Chemistry and Abbe Center of Photonics, Helmholtzweg 4, 07743 Jena, Germany

<sup>3</sup> InfectoGnostics Research Campus Jena, Centre for Applied Research, Philosophenweg 7, 07743 Jena, Germany

<sup>4</sup> Laboratorio de Bioinformática y Biología Molecular, Facultad de Ciencias, Universidad Peruana Cayetano Heredia, Lima 31, Peru; patricia.sheen@upch.pe (P.S.); mirko.zimic@upch.pe (M.Z.)

\* Correspondence: dana.cialla-may@leibniz-ipht.de; Tel.: +49-3641-206-309

† These Authors contributed equally.

‡ Current address: CiS Forschungsinstitut für Mikrosensorik GmbH, Konrad-Zuse-Straße 14, 99099 Erfurt, Germany.

Received: 15 February 2019; Accepted: 29 May 2019; Published: 20 June 2019



**Featured Application:** With the presented microfluidic LoC-SERS device, it is possible to detect simultaneously the prodrug pyrazinamide (PZA) and its metabolite pyrazinoic acid (POA). Thus, our proposed detection scheme could be used for an indirect detection of PZA resistance in *Mycobacteria tuberculosis* culture supernatants.

**Abstract:** The prodrug pyrazinamide (PZA) is metabolized by the mycobacteria to pyrazinoic acid (POA), which is expelled into the extracellular environment. PZA resistance is highly associated to a lack of POA efflux. Thus, by detecting a reduction of the concentration of POA in the extracellular environment, by means of lab-on-a-chip (LoC)-SERS (surface-enhanced Raman spectroscopy), an alternative approach for the discrimination of PZA resistant mycobacteria is introduced. A droplet-based microfluidic SERS device has been employed to illustrate the potential of the LoC-SERS method for the discrimination of PZA resistant mycobacteria. The two analytes were detected discretely in aqueous solution with a limit of detection of 27  $\mu\text{M}$  for PZA and 21  $\mu\text{M}$  for POA. The simultaneous detection of PZA and POA in aqueous mixtures could be realized within a concentration range from 20  $\mu\text{M}$  to 50  $\mu\text{M}$  for PZA and from 50  $\mu\text{M}$  to 80  $\mu\text{M}$  for POA.

**Keywords:** surface-enhanced Raman spectroscopy (SERS); personal medicine; drug resistant mycobacteria; quantitative SERS detection of PZA and POA; lab-on-a-Chip (LoC)

## 1. Introduction

Tuberculosis (TB) is a disease affecting 10.0 million people globally each year [1], with drug resistance becoming a growing threat. TB remains one of the major causes of disease and death

worldwide, exacerbated by HIV-TB co-infection [2] and the emergence of multidrug-resistant (MDR) and extensively drug resistant (XDR) TB strains in both industrialized and developing countries [2,3]. TB is a curable disease; however, the mortality rate associated with this medical condition has considerably increased during the last years. The newly emerging MDR mycobacteria strains lead to a doubling of the MDR TB cases that are hard to treat. The early and correct identification of the drug susceptibility of the TB strain affecting a patient is crucial for a positive anti-tuberculous treatment outcome.

Drug susceptibility testing for *Mycobacterium tuberculosis* (MTB) can be performed with various assays, such as the radiometric BACTEC 460TB method [4,5], the automated non-radiometric mycobacteria growth indicator tube (MGIT) 960 system [6–8] and the microtiter-based alamar blue assay [9,10], among others. Phenotypic assays based on cell cultures in Löwenstein–Jensen dry medium are still considered to be the gold standard [11,12]. Nevertheless, mycobacteria present a slow growth under dry conditions and the time for the result of the later assay can take up to three weeks for detection and an additional two to three weeks for drug susceptibility testing. Furthermore, although in high income countries the available financial resources assure the access for the patients to optimal diagnosis and individualized treatment schemes, in low resource regions, MDR-TB and XDR-TB cases with medical care requirements extending up to two years are hard to assess and treat. In the search for cost and time effective assays, the microscopic observation drug susceptibility (MODS) testing was introduced more than 15 years ago [13,14]. Even though the MODS testing requires highly trained personnel, the necessary laboratory infrastructure is reduced to a centrifuge, an incubator and an inverted microscope. Furthermore, bacteria are cultured in sealed containers under liquid conditions assuring optimal growth conditions and providing information on drug susceptibility in less than two weeks [15].

The most common first line agents administered for drug-susceptible TB are rifampicin, isoniazid, ethambutol and pyrazinamide (PZA) [16]. PZA is the only drug with different activity in vivo and in vitro [17]. Its importance is based on its in vivo sterilizing effect that permits killing of persistent bacilli [18]. PZA is frequently used in both first- and second-line treatment regimens [19–21]. The incorporation of PZA into TB treatment regimens in the 1960s enabled the duration of first-line treatment to be reduced from nine to 12 months down to six months [22]. Among the drugs rifampicin, isoniazid, ethambutol and PZA, PZA susceptibility testing is the most challenging and it is not routinely performed [23–25]. The compound itself is not active against mycobacteria. It is administered as a pro-drug and its metabolite, pyrazinoic acid (POA), kills semi-dormant MTB in the acidic regions of acute inflammation that are inaccessible to other anti-TB drugs [22,24,26].

The conversion of the pro-drug to the metabolite is realized by the bacterial enzyme nicotinamidase/pyrazinamidase. The known major mechanism of PZA resistance is associated with a mutation of the pyrazinamidase enzyme resulting in no or a very low conversion rate to POA. Therefore, an indirect way of assessing PZA resistance is to determine the presence of POA in the extracellular environment of an in vitro liquid culture in the presence of PZA, such as the MODS-Wayne assay [27]. Colorimetric methods based on the reaction between ammonium iron sulfate and POA have been employed in order to assess the presence of the metabolite in the culture and to confirm the enzyme activity [27,28]. Although the colorimetric method is straight forward, it offers only pure qualitative information. On the other side, chromatography based methods have been also used for quantifying PZA and POA in biological fluids [29–31]. Nevertheless, for routine high throughput analysis chromatographic methods are unpractical and cost intensive.

As an alternative analytical tool Raman spectroscopy-based methods are very promising approaches. Raman spectroscopy is suitable for the fingerprint specific detection of low molecular weight substances, such as PZA and POA. It provides a specific and unique spectroscopic pattern. Combining Raman spectroscopy with plasmonic nanoparticles (NPs) the surface-enhanced Raman spectroscopy (SERS) enables us to detect very low concentrations of target analytes. Thus, SERS is well known to offer sensitive and specific information on the molecular level [32,33]. With the advent of miniaturized, low cost Raman setups and the development of in situ synthesis protocols, SERS is considered to have a high potential for clinical applications [34,35]. The combination of SERS

with microfluidics offers an attractive method (lab-on-a-chip SERS, LoC-SERS). The application of a microfluidic flow-through device allows for a high throughput measurement protocol employing small sample volumes. Thus, a large data set can be achieved in a short time frame. Furthermore, the microfluidic environment ensures a very stable and easy to reproduce measurement conditions.

The majority of the antecedent investigation of PZA and its metabolite POA applying Raman spectroscopy focused on the vibrational assignment of the theoretical determined spectral positions of the Raman bands of these two molecules [36–38]. However, only few efforts were made so far to investigate PZA or POA by means of SERS [39–41].

Within this study, we aim for the molecular specific and sensitive detection of the target molecules PZA and POA employing SERS as an analytical tool. To the best of our knowledge, this is the first study focusing on the simultaneous determination of PZA and its metabolite POA within a droplet-based lab-on-a-chip SERS (LoC-SERS) platform using in situ synthesized silver NPs. Thus, in this proof of principle study the detection and discrimination of the two molecules in one approach is addressed and the potential of the ratiometric detection scheme is evaluated for the determination of PZA resistance in MTB isolates.

## 2. Materials and Methods

### 2.1. Materials and Samples

Pyrazinamide (PZA, 97.5%), pyrazinoic acid (POA, 99%), AgNO<sub>3</sub> (99.9999% trace metals basis), hydroxylamine hydrochloride (99.999% trace metals basis), hydrazine monohydrate (64–65%, reagent grade, 98%), sodium citrate (ACS reagent, ≥99.0%) and chile salpeter (NaNO<sub>3</sub>, ≥99.0%) were purchased from Sigma Aldrich, Darmstadt, Germany and used as received. Ammonia solution (32%) and sodium hydroxide (≥98%, Ph.Eur.) were purchased from Carl Roth, Karlsruhe, Germany and used as received. Stock solutions at a given concentration were prepared by adding the appropriate amount of powder to high purity water in the case of PZA, POA and sodium citrate.

### 2.2. Microfluidic Flow Cell

An all-glass microfluidic device, in house designed for SERS measurements [42], was used for the LoC-SERS experiments. It combines multi-fluid injectors (Ismagilow injector) [43] and meandering mixing channels, segment flow creation and dosing nozzles [44] and a long measuring channel loop to record the SERS spectra. To permit for a variety of photonic applications in analytics the optical transparent microchannels are prepared employing the technology of wet etching and anodic bonding of two glass substrates using a bond-support layer. To realize the different etching depths within one single substrate a two-step etching process was applied. Subsequently, the microchannels were prepared with channel dimensions of 560 μm<sup>2</sup> × 260 μm<sup>2</sup>. The so called ideal minimum compartment volume (IMCV) [45] was defined to be 55 nL for the SERS measurements of aqueous/tetradecane two-phase flows. The meandering channels have a radius of 500 μm. Each loop of the measurement channel has a length of 10.900 μm. The surface of the microchannels is functionalized with octadecyltrichlorosilane (ODTS) in order to achieve optimum wettability for the continuous phase and minimum wettability for the aqueous droplets. For the surface modification the bond-support layer has been removed from microchannels by a treatment with 5 mol/L NaOH in water at 80 °C for 5 min. Subsequently, the channels were washed with 1 mol/L NaOH and water. The activation of the channel surface was realized by a treatment with piranha solution followed by a drying step at 120 °C. The final surface functionalization was achieved by treatment with a solution of 5 mmol/L octadecyltrichlorosilane in anhydrous tetradecane at 60 °C for 4 h.

### 2.3. Batch Synthesis of the Nanoparticles—h-AgNPs

For the spectral characterization of PZA and POA in cuvette measurements, batch-synthesized AgNPs were used. Hydroxylamine hydrochloride reduced silver nanoparticles h-AgNPs were

synthesized following the Leopold–Lendl protocol [46]. Briefly, a volume of 10 mL solution containing 0.1 mmol silver nitrate was added to 90 mL solution containing 0.3 mmol sodium hydroxide and 1.5 mmol hydroxylamine hydrochloride under rigorous steering. A yellow colloidal solution containing silver nanoparticles, stable over few weeks, was obtained.

#### 2.4. *In Situ Synthesized Nanoparticles— $\gamma$ -AgNPs*

In order to achieve controllable and reproducible synthesis conditions, the strategy already described by Dugandžić et al. [47] was employed within this study. A segmented flow microfluidic chip illustrated in Figure S1 in the Supplementary Information (SI) was used for both nanoparticle synthesis and SERS measurements in the same time. An aqueous mixture containing  $\text{AgNO}_3$  (3 mM) and  $\text{NH}_3$  (15 mM) was injected with a flow rate of 20 nL/s via port 2, 10  $\mu\text{M}$  concentrated sodium citrate solution was provided through port 3 with 5 nL/s flow velocity, while 1.5 mM  $\text{N}_2\text{H}_4$  (reducing agent) was pumped in via port 4 with a flow rate of 20 nL/s. The in situ silver nanoparticle  $\gamma$ -AgNPs are generated in the main channel of the microfluidic chip. Before and after each measurement series, the droplet generator, including port 1, 2 and 3, was flushed with the citrate solution ( $10^{-5}$  M) with a flowrate of 500 nL/s to avoid blocking of the channels.

#### 2.5. *Instrumentation and Measurements*

Raman and SERS spectra were recorded with a fiber coupled commercial Raman setup from WITec GmbH, Ulm, Germany. For excitation, a diode laser (Fandango, Cobolt, Kassel, Germany) with an emission wavelength at 514 nm was used. The same objective (20 $\times$ , 0.4 N.A., Zeiss, Jena, Germany) was applied to focus the laser beam on the surface of the sample and to collect the backscattered photons. For recording the reference Raman spectrum of PZA 20 mW and for POA 5 mW laser power was incident on the sample, respectively. For all SERS measurements, 40 mW laser power was applied. For detection, a thermoelectrically cooled CCD (1024  $\times$  127) camera and a 600 l/mm grating with a spectral resolution of  $\sim 5\text{ cm}^{-1}$  were used.

For Raman measurements on powder, a small amount of the sample was placed on a conventional microscope glass slide. Spectra were acquired with a 1 s integration time and 10 accumulations. SERS spectra in cuvettes (BRAND<sup>®</sup> 96-well PCR plate from Sigma Aldrich, Darmstadt, Germany) were measured after mixing equal amounts of colloidal h-AgNPs (100  $\mu\text{L}$ ) with the sample solution (100  $\mu\text{L}$ ) and adding additional high purity water or an aggregation agent (20  $\mu\text{L}$ ). For aggregation  $\text{NaNO}_3$  was used at the concentration of 0.5 M. Each spectrum is the result of 10 accumulations of spectra recorded with an integration time of 1 s.

LoC-SERS measurements were carried out by mounting a droplet based microfluidic chip (Figure S1) on the microscope table of the Raman setup. For injecting the solutions into the chip a computer controlled nMESYS pump system from Cetoni GmbH, Gera, Germany was employed and glass syringes purchased from ILS GmbH, Stützerbach, Germany with 250, 500 and 2500  $\mu\text{L}$  volumes were used. The syringes were connected to the chip with teflon capillaries (inner diameter of 0.5 mm; Wicom GmbH, Heppenheim, Germany). If not otherwise stated, the flow rates were set as follows: 20 nL/s for mineral oil,  $\text{AgNO}_3/\text{NH}_3$  and  $\text{N}_2\text{H}_4$ , each. For the sodium citrate solution: 5 nL/s; and 40 nL/s in total for the two ports providing the sample and the aggregation agent ( $\text{NaNO}_3$ ). The controlled aggregation of metallic nanoparticles during the SERS analysis is beneficial to create hot spots. Due to the very well-controlled environment generated in the microfluidic chip the application of agglomeration agents can be very helpful to achieve high signal intensity in the SERS spectra. The spectra were continuously recorded during the dynamic flow with a 0.5 s integration time. The number of spectra for each measurement, if not otherwise stated, was 1200.

#### 2.6. *Data Analysis*

The recorded Raman and SERS spectra were pre-processed and analyzed with in-house written algorithms (GnuR) [48]. The reference Raman and SERS spectra were background corrected with the

selective nonlinear iterative peak clipping (SNIP) method [49] and cut to the 200–1650  $\text{cm}^{-1}$  fingerprint region and 2800–3300  $\text{cm}^{-1}$  CH stretching region. Due to the motion of the sample containing droplets no thermal (burning) effects were observed.

The spectra recorded with the LoC-SERS device were separated into two groups by k-means cluster analysis. One group contains the mineral oil spectra, the other one contains the pure droplet SERS spectra. This was followed by a wavenumber calibration, where mineral oil was used as a standard [50]. Afterward, stacks of three spectra recorded within one droplet were averaged, background corrected (SNIP, 45 iterations) and cut to the wavenumber region of interest.

### 3. Results

#### 3.1. PZA and POA: Spectral Characterization

Raman spectroscopy is known to provide highly specific signals and to allow the discrimination of molecules based on the achieved information in the vibrational spectra. POA is the active metabolite of PZA, its absence or presence in a very low amount in *in vitro* MT cell cultures after the administration of PZA might indicate PZA resistance of the bacteria culture. Therefore, it is essential to implement an analytical method for the analysis and accurate detection of POA alone or POA/PZA mixtures and discriminate this from samples containing just the prodrug PZA. The two targeted substances are structurally very similar molecules (Figure 1). Both share a pyrazine ring, whereas PZA has an amide moiety and POA a carboxylic acid group. This is why, the reference Raman spectra measured on the pure powder (Figure 1a,b; gray spectra at the bottom) show besides some common bands also several modes specific for each molecule. The detailed assignment of the Raman bands has been already reported in the literature [37,38,40,41]. The marker bands for the pyrazine ring are the doublet present in the spectrum of both molecules at 1021 and 1055  $\text{cm}^{-1}$  corresponding to the in-plane bending of the pyrazine ring and the CN stretching mode of the same ring at 1528  $\text{cm}^{-1}$ . In the high wavenumber range the mode of the CH stretching vibrations arises at 3066  $\text{cm}^{-1}$ . Specific marker bands for PZA are the band at 1080  $\text{cm}^{-1}$  (rocking of the  $\text{NH}_2$  group) and the band at 1440  $\text{cm}^{-1}$  (bending of the  $\text{NH}_2$  group). The significant marker band for POA is located around 1710  $\text{cm}^{-1}$ , ascribed to the C=O stretching of the carboxylic moiety.

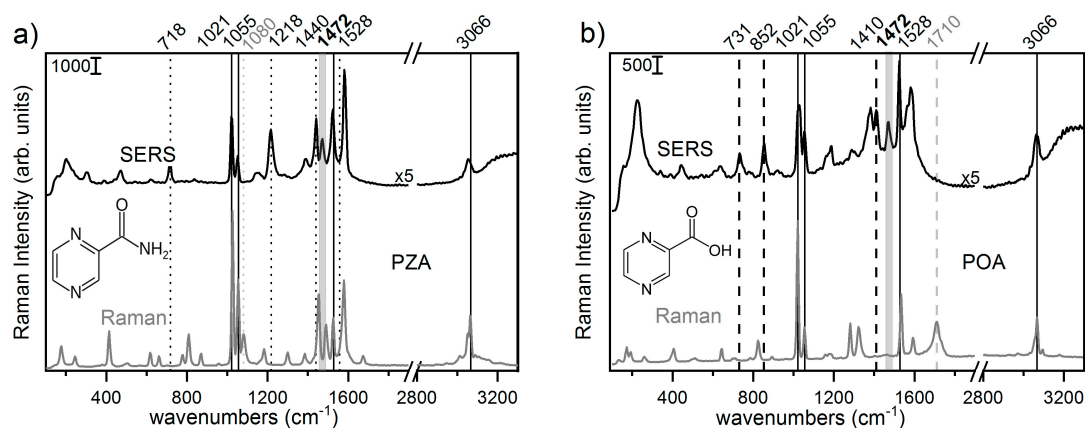


**Figure 1.** Reference Raman spectra of the powder (gray spectra in the bottom) and surface-enhanced Raman spectroscopy (SERS) spectra (black spectra in the top), applying hydroxyl amine hydrochloride reduced h-AgNPs, of PZA and POA in a concentration of  $10^{-3}$  M in panel (a) and (b), respectively. Marker bands for both analytes are indicated with black lines, marker band specific for PZA are depicted with dotted lines, marker band for POA with dashed lines. For both analytes a scheme of the molecular structure is shown.

Although Raman spectroscopy provides a very high specificity, the sensitivity that is required for the discrimination of PZA susceptible and PZA resistant MTB can only be achieved by enhancing

the Raman signal. However, exploiting the plasmon-based surface enhancement effect, the presence of plasmonic NPs can significantly change the spectral profile of the SERS spectra as compared to the Raman spectra. This is associated with surface dependency effects, e.g., orientation to the surface (surface selection rules), gradient field effect and charge-transfer events, which results in variations of the spectral position and/or intensity of certain peaks [51,52]. In the SERS spectrum of PZA and POA (aqueous solution, concentration  $10^{-3}$  M, h-AgNP) measured with hydroxyl amine hydrochloride reduced batch silver nanoparticles h-AgNPs (Figure 1a,b) top panel) the three Raman modes characteristic for the fundamental vibrations of the pyrazine ring ( $1021\text{ cm}^{-1}$ ,  $1055\text{ cm}^{-1}$  and  $1528\text{ cm}^{-1}$ ) are still clearly visible and unaffected by the proximity of the silver surface.

For PZA, a new band caused by the symmetric stretching of the amide group of the pyrazine ring appears in the SERS spectra at  $1218\text{ cm}^{-1}$  [53]. Furthermore, the signal centered at  $718\text{ cm}^{-1}$  in the SERS spectra is assigned to the OCN bending vibration. Considering the observed changes in the SERS-spectra as compared to the Raman spectra and the surface selection rules it is possible to assume the orientation of the PZA molecules relative to the surface. Most likely the interaction takes place through the nitrogen atom, resulting in the upright position of the aromatic ring structure relative to the metal surface. Therefore, the symmetric stretching of the amide group of the pyrazine ring appears in the SERS spectra at  $1218\text{ cm}^{-1}$ . This observation is in accordance with an investigation of pyridine derivatives providing similar molecular structure [52].

For POA the band appearing at  $1410\text{ cm}^{-1}$  in the SERS spectra is caused by the vibration of the carboxylate group [41]. Furthermore, dominant modes in the SERS spectra of POA are appearing at  $731\text{ cm}^{-1}$  (OCO out-of-plan bending) and  $852\text{ cm}^{-1}$  (ring breathing). For a detailed band assignment, the reader is referred to Table S1 (Supplementary Information). Due to the observed changes in the SERS spectra as compared to the Raman spectra it is suggested that the POA molecules are interacting with the metal surface through the nitrogen of the pyrazine ring. In the POA SERS spectra the OCO vibration mode and the ring breathing mode are more enhanced pointing to an upright orientation of the pyrazine ring relative to the metal surface.

The discussed spectral differences allow for the discrimination of the two structurally similar molecules based on their SERS spectra in a complex matrix.

### 3.2. Optimization of the SERS Measurement Conditions

Using metallic nanoparticles in an aqueous solution for the SERS measurements, issues associated with batch-to-batch compatibility and aging effects are well known. Thus, to prevent the mentioned obstacles an in situ approach for the AgNP production is suitable. For this purpose, the microfluidic platform, established by März et al. [42], provides the required preparation conditions. A constant volume flow allows for very precise mixing ratios. This is combined with the possibility to mix and add substances separately, ensuring for perfect mixing conditions. Furthermore, the long measuring unit enables variation of the reaction time in order to optimize the signal intensity. For the in situ production of AgNPs in a microfluidic chip device, the Lee–Meisel protocol [54] is not suitable because of the synthesis requirements of boiling under reflux conditions for over one hour. The Leopold–Lendl protocol [46] instead can be realized under room temperature conditions and on a time scale shorter than one minute [55]. However, the required sodium hydroxide would react with the hydrophobic silane layer on the glass surface of the microfluidic chip and at the same time inhibit the successful creation of droplets as well as the nanoparticles. As an alternative method, hydrazine can be used as reduction agent in the presence of a low amount of citrate to synthesize  $\gamma$ -AgNPs in the applied microfluidic chip device [47].

When large batch protocols are transferred to microfluidic platforms new degrees of freedom, such as flow rates or time elapsed from substance mixing to measurement, arise. Thus, the production protocol needs to be adapted in order to control the order of addition and the concentration of the reagents in the mixture. As POA is the main targeted analyte, the influence of the flow rates and the addition of citrate as a stabilizing agent were investigated in order to establish the ideal measurement

conditions. Generally, a proper and reproducible mixing of reagents during in situ colloid synthesis is essential to achieve reliable SERS results. In order to synthesize the hydrazine reduced silver NPs in the microfluidic chip three initial reagents are needed: An aqueous solution containing 3 mM  $\text{AgNO}_3$  and 15 mM  $\text{NH}_3$  (flowrate: 5–30 nL/s), an aqueous solution of 1.5 mM  $\text{N}_2\text{H}_4$  (flowrate: 5–30 nL/s) and an aqueous solution of the stabilizing agent sodium citrate with the concentration of  $10^{-5}$  M (flowrate: 5 nL/s) are inserted to the chip at the droplet generator unit. For the experiment the flowrate of mineral oil (separation media) was varied between 5 and 30 nL/s, while the flowrates of POA and the aggregation agent (0.5 M  $\text{Na}_2\text{SO}_4$ ) were kept constant at 10 nL/s each. The mean of the measured spectra for the varying flowrates are depicted in Figure 2.

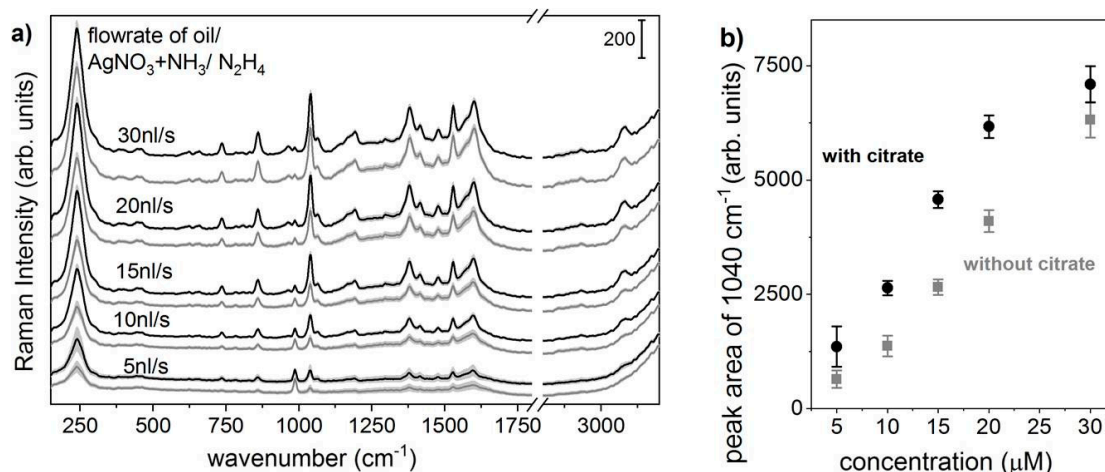


**Figure 2.** (a) Varying flowrates for mineral oil,  $\text{AgNO}_3$  with  $\text{NH}_3$  and  $\text{N}_2\text{H}_4$  in the microfluidic chip device. The flowrates of PZA ( $10^{-4}$  M) and  $\text{NaNO}_3$  were kept constant at 10 nL/s. With the addition of citrate ( $10^{-5}$  M) depicted in black, without citrate plotted in gray. In light gray the standard deviation values are indicated. (b) Integrated intensity of the peak at  $1040 \text{ cm}^{-1}$  relative to the different flowrates. With addition of citrate ( $10^{-5}$  M) depicted in black, without citrate plotted in gray, respectively.

It was found, that the optimized environment for a good signal to noise ratio and high intensity of the SERS spectra is achieved when citrate was added (5 nL/s) and the flowrates of mineral oil,  $\text{AgNO}_3/\text{NH}_3$  solution and  $\text{N}_2\text{H}_4$  was set to 30 nL/s. This might be attributed to better mixing conditions of the reagents due to the increased flow velocity. In a next step, after the reduction of silver nitrate was completed, the analyte was injected into the droplet through the dosing unit and pure SERS spectra of the analyte molecules were recorded with a very good signal-to-noise ratio. In general, a triple determination is required to achieve a reliable data set. Subsequently, three spectra were measured in every droplet (integration time 0.5 s) and the average spectrum was estimated.

### 3.3. Quantitative Detection of PZA and POA Applying the LoC-SERS Device

The presence of PZA resistant MTB in patient samples can be deduced from the absence of POA in the in vitro cell cultures. The amount of PZA added to these assays is not standardized. For example, in a quantitative Wayne assay PZA concentrations were set to 400  $\mu\text{g}/\text{mL}$  (3.2 mM) and 800  $\mu\text{g}/\text{mL}$  (6.4 mM) [56], whereas in another test 100  $\mu\text{g}/\text{mL}$  (0.8 mM) PZA was used as a critical concentration. In order to determine whether the bacterial culture is susceptible or resistant to PZA using SERS as analytical tool, the limit of detection (LOD) of the prodrug and its metabolite needed to be identified in a first step. Thus, both analytes were dissolved in high purity water. For each analyte a stock solution of 0.1 mM was achieved and diluted to lower concentrations ranging from 100  $\mu\text{M}$  to 2  $\mu\text{M}$ . A flow profile was applied to vary the in-chip concentration during the measurements in the microfluidic device (detailed flow rates are given in the instrumentation and measurement section and SI). The background signal of the in situ synthesized colloids ( $\gamma$ -AgNPs) shows some weak bands that can be ascribed to

the sodium citrate used as stabilization agent (Figures 3 and 4: background spectra depicted in gray). The LOD was determined employing the three times standard deviation value of the background signal as a threshold ( $3\sigma$ ). For both analytes the SERS signal vs. concentration yields a sigmoidal curve, which is well known to be characteristic for the SERS technique due to saturation at high concentrations. The calculated limit of detection for PZA is  $27 \mu\text{M}$ , while for POA  $21 \mu\text{M}$  (see Figure S2 in the SI for more details).

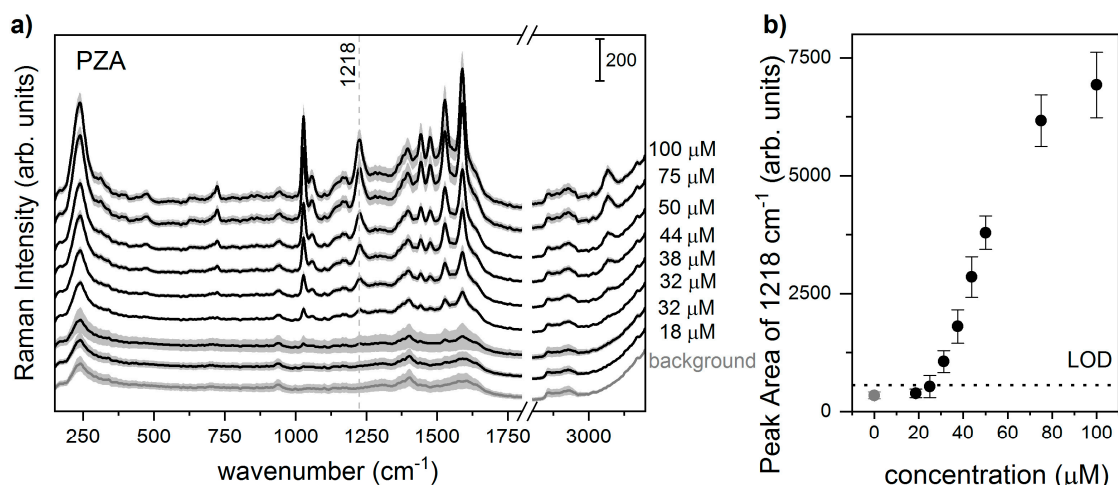


**Figure 3.** (a) Lab-on-a-chip SERS (LoC-SERS) mean spectra of different concentrated PZA in water as indicated in the plot. The standard deviation values are indicated in grey; (b) the integrated intensity of the marked peak centered at  $1218 \text{ cm}^{-1}$ .

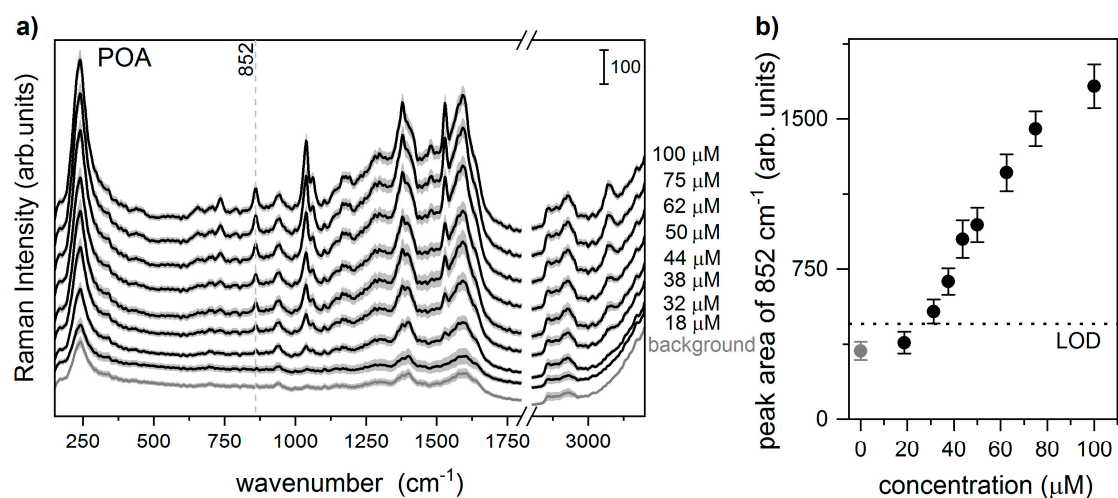


**Figure 4.** (a) LoC-SERS mean spectra of different concentrated POA in water as indicated in the plot. The standard deviation values are indicated in grey; (b) the integrated intensity of the marked peak centered at  $852 \text{ cm}^{-1}$ .

### 3.4. Simultaneous Detection of PZA and POA in Aqueous Solution

To prove the high potential of the LoC-SERS device for providing reliable data for the PZA resistance discrimination, first PZA and POA were detected simultaneous in an aqueous solution. In the supernatant of the PZA treated mycobacteria only PZA might be found in the case of PZA resistance. However, if the bacteria are PZA susceptible a mixture of PZA and POA will be found in the supernatant. Therefore, depending on the conversion rate of PZA to POA, the time of analysis and presence of PZA resistance, POA might be present in a mixture with PZA or might be completely absent. Consequently, it is of interest to discriminate between samples containing only PZA, a mixture

of PZA and POA and only POA. As a proof of principle, samples with different prodrug-metabolite ratios were measured. As discussed above, the two molecules show, besides common bands ascribed to the vibrations of the pyrazine ring, also vibrational modes characteristic for the different analytes. It is expected that these differences in the SERS spectra will also be visible in a mixture. Seven different mixtures were measured using the LoC-SERS setup, the concentration of PZA ranging from 0 to 100  $\mu\text{M}$  and the concentration of POA from 100 to 0  $\mu\text{M}$ . The means of the measured SERS spectra are depicted in Figure 5a. Differences are obvious in band intensity ratios, positions and the presence/absence of the specific marker bands.

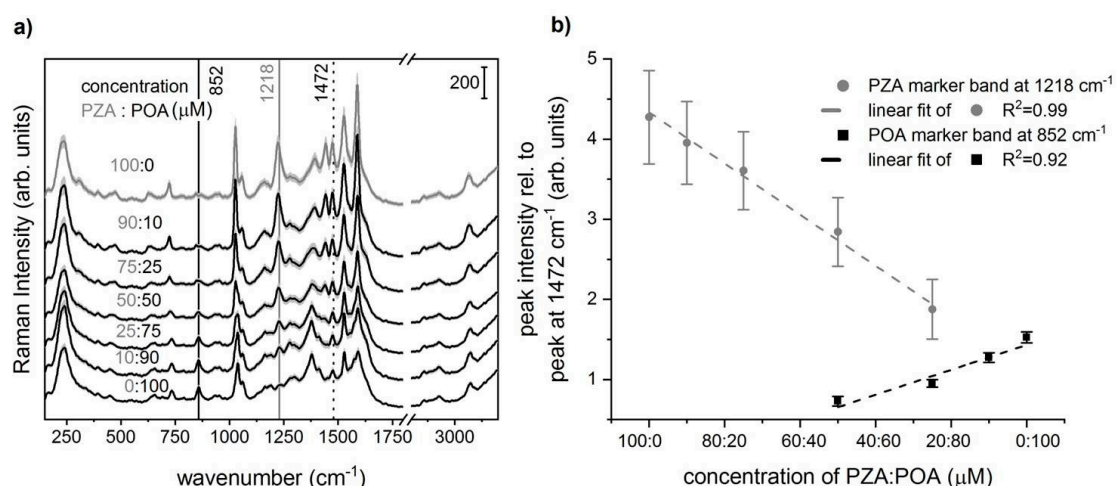


**Figure 5.** (a) LoC-SERS mean spectra of mixtures of PZA (gray) and POA (black) in water (using  $\gamma$ -AgNPs). Mixing ratios of analyte stock solutions ( $10^{-4}$  M) are indicated in the graph. Mixing was realized before injection into the chip. The standard deviation values are indicated in light gray; (b) peak intensities of the marker bands at  $1218\text{ cm}^{-1}$  (for PZA) and  $852\text{ cm}^{-1}$  (for POA) relative to the peak at  $1472\text{ cm}^{-1}$ , respectively.

The mayor differences can be noticed in bands located at  $852$  and  $1372\text{ cm}^{-1}$  characteristic for POA and the vibrational modes centered at  $1218$  and  $1440\text{ cm}^{-1}$ , being marker modes for PZA. These bands are changing in ratio correlated to the individual concentrations of both target molecules. In Figure 5b, the peak intensity of the PZA marker mode at  $1218\text{ cm}^{-1}$  and the POA marker mode at  $852\text{ cm}^{-1}$  are plotted after normalization to the peak at  $1472\text{ cm}^{-1}$ . The reference band centered at  $1472\text{ cm}^{-1}$  is caused by N–C stretching [38]. This band is present in the spectra of both analytes (as indicated in Figure 1a,b) with a resembling intensity. Thus, this band is very well suited as a reference band for the normalization. For both analytes a linear signal to concentration dependency could be observed. For PZA the concentration ranged from 20 to 100  $\mu\text{M}$  (with a coefficient of correlation  $R^2 = 0.99$ ) and for POA the range from 50 to 100  $\mu\text{M}$  (with a coefficient of correlation  $R^2 = 0.92$ ) could be determined. Thus, for the concentration PZA/POA 20  $\mu\text{M}$ /80  $\mu\text{M}$  to 50  $\mu\text{M}$ /50  $\mu\text{M}$  to simultaneous detection could be realized as very successful. The detection limits for PZA and POA are 20  $\mu\text{M}$  and 50  $\mu\text{M}$ , respectively.

#### 4. Discussion

In the present work, the potential of LoC-SERS as a spectroscopic based method was demonstrated for the simultaneous detection of PZA and POA in a microfluidic device. The significant differences in the SERS spectra of PZA and POA were determined, e.g., for PZA specific marker bands are centered at  $1218\text{ cm}^{-1}$  and  $718\text{ cm}^{-1}$ , for POA the marker bands are centered at  $731\text{ cm}^{-1}$  and  $852\text{ cm}^{-1}$ . The flow rates in the microfluidic device could be optimized to achieve best signal to noise ratio when citrate (concentration  $10^{-5}\text{ M}$ ) was added (5 nL/s) and the flowrates of mineral oil,  $\text{AgNO}_3/\text{NH}_3$  solution and  $\text{N}_2\text{H}_4$  was set to be 30 nL/s, while analyte flowrate was set to 10 nL/s.

In aqueous conditions for both analytes the SERS signal vs. concentration yields a sigmoidal curve. However, the limit of detection was calculated to be 27  $\mu\text{M}$  for PZA and 21  $\mu\text{M}$  for POA when detected discretely each one. Thus, it could be shown as a proof of principle that the discrimination between PZA and its metabolite POA can be realized with a very high sensitivity. Furthermore, the two analytes were simultaneously detected in aqueous solution with varying concentrations, it was demonstrated that a linear dependency of the Raman signal with respect to the concentration holds true in the range of 20  $\mu\text{M}$  to 100  $\mu\text{M}$  for PZA and 50  $\mu\text{M}$  to 100  $\mu\text{M}$  for POA, respectively. The detection limits for PZA and POA in a mixture of both analytes are 20  $\mu\text{M}$  and 50  $\mu\text{M}$ , respectively. The ratio of the marker modes of PZA and POA can be a relevant indicator for PZA resistant MTB.

**Supplementary Materials:** The following are available online at <http://www.mdpi.com/2076-3417/9/12/2511/s1>, Figure S1: Droplet based microfluidic chip, Figure S2: Determination for the limit of detection for PZA and POA solved in high purity water, Table S1: band assignment for PZA and POA according to the cited literature, Measurement overview.

**Author Contributions:** Conceptualization, I.J.J., P.S., M.Z. and D.C.-M.; Formal analysis, A.M., M.J.; Funding acquisition, M.Z. and D.C.-M.; Investigation, J.H. and P.S.; Methodology, A.M.; Project administration, K.W. and D.C.-M.; Supervision, J.P.; Writing—original draft, A.M. and I.J.J.; Writing—review & editing, K.W., P.S., M.Z., D.C.-M. and J.P.

**Funding:** We gratefully acknowledge the Federal Ministry of Education and Research, Germany (BMBF) for supporting the InfectoGnostics (13GW0096F) and EXASENS (13N13856) project grants as well as BMBF and German Aerospace Center (DLR) for supporting the Myco-NET2 (01DN15028) project grant. We thank for funding the projects ERANET LAC ELAC2014/HID-0352, CONCYTEC-FONDECYT-Peru 086-2015, and the Wellcome Trust Intermediate Fellowship (grant 099805/Z/12/Z).

**Conflicts of Interest:** The authors declare no conflict of interest. The funders had no role in the design of the study; in the collection, analyses, or interpretation of data; in the writing of the manuscript, or in the decision to publish the results.

## References

1. *Global Tuberculosis Report 2018*; World Health Organization: Geneva, Switzerland, 2018.
2. Corbett, E.L.; Watt, C.J.; Walker, N.; Maher, D.; Williams, B.G.; Raviglione, M.C.; Dye, C. The growing burden of tuberculosis: Global trends and interactions with the hiv epidemic. *Arch. Internal Med.* **2003**, *163*, 1009–1021. [[CrossRef](#)] [[PubMed](#)]
3. Raviglione, M.C.; Gupta, R.; Dye, C.M.; Espinal, M.A. The burden of drug-resistant tuberculosis and mechanisms for its control. *Ann. N.Y. Acad. Sci.* **2001**, *953b*, 88–97. [[CrossRef](#)] [[PubMed](#)]
4. Somoskovi, A.; Kodmon, C.; Lantos, A.; Bartfai, Z.; Tamasi, L.; Fuzy, J.; Magyar, P. Comparison of recoveries of mycobacterium tuberculosis using the automated bactec mgit 960 system, the bactec 460 tb system, and lowenstein-jensen medium. *J. Clin. Microbiol.* **2000**, *38*, 2395–2397. [[PubMed](#)]
5. Roggenkamp, A.; Hornef, M.W.; Masch, A.; Aigner, B.; Autenrieth, I.B.; Heesemann, J. Comparison of mb/bact and bactec 460 tb systems for recovery of mycobacteria in a routine diagnostic laboratory. *J. Clin. Microbiol.* **1999**, *37*, 3711–3712. [[PubMed](#)]
6. Hillemann, D.; Richter, E.; Rusch-Gerdes, S. Use of the bactec mycobacteria growth indicator tube 960 automated system for recovery of mycobacteria from 9,558 extrapulmonary specimens, including urine samples. *J. Clin. Microbiol.* **2006**, *44*, 4014–4017. [[CrossRef](#)]
7. Marttila, H.J.; Marjamaki, M.; Viljanen, M.K.; Soini, H. Performance of bactec 960 mycobacteria growth indicator tube in the susceptibility testing of genetically characterized mycobacterium tuberculosis isolates. *Eur. J. Clin. Microbiol. Infect. Dis.* **2003**, *22*, 757–759. [[CrossRef](#)]
8. Bemer, P.; Palicova, F.; Rusch-Gerdes, S.; Drugeon, H.B.; Pfyffer, G.E. Multicenter evaluation of fully automated bactec mycobacteria growth indicator tube 960 system for susceptibility testing of mycobacterium tuberculosis. *J. Clin. Microbiol.* **2002**, *40*, 150–154. [[CrossRef](#)]
9. Reis, R.S.; Neves, I.; Lourenco, S.L.S.; Fonseca, L.S.; Lourenco, M.C.S. Comparison of flow cytometric and alamar blue tests with the proportional method for testing susceptibility of mycobacterium tuberculosis to rifampin and isoniazid. *J. Clin. Microbiol.* **2004**, *42*, 2247–2248. [[CrossRef](#)]
10. Chauca, J.A.; Palomino, J.C.; Guerra, H. Evaluation of the accuracy of the microplate alamar blue assay for rapid detection of mdr-tb in peru. *Int. J. Tuberc. Lung Dis.* **2007**, *11*, 820–822.

11. Kohli, A.; Bashir, G.; Fatima, A.; Jan, A.; Wani, N.-U.-D.; Ahmad, J. Rapid drug-susceptibility testing of mycobacterium tuberculosis clinical isolates to first-line antitubercular drugs by nitrate reductase assay: A comparison with proportion method. *Int. J. Mycobacteriol.* **2016**, *5*, 469–474. [[CrossRef](#)]
12. Van Deun, A.; Aung, K.J.M.; Bola, V.; Lebeke, R.; Hossain, M.A.; de Rijk, W.B.; Rigouts, L.; Gumusboga, A.; Torrea, G.; de Jong, B.C. Rifampin drug resistance tests for tuberculosis: Challenging the gold standard. *J. Clin. Microbiol.* **2013**, *51*, 2633–2640. [[CrossRef](#)]
13. Caviedes, L.; Lee, T.S.; Gilman, R.H.; Sheen, P.; Spellman, E.; Lee, E.H.; Berg, D.E.; Montenegro-James, S.; Tuberculosis Working Grp, P. Rapid, efficient detection and drug susceptibility testing of mycobacterium tuberculosis in sputum by microscopic observation of broth cultures. *J. Clin. Microbiol.* **2000**, *38*, 1203–1208. [[PubMed](#)]
14. Park, W.G.; Bishai, W.R.; Chaisson, R.E.; Dorman, S.E. Performance of the microscopic observation drug susceptibility assay in drug susceptibility testing for mycobacterium tuberculosis. *J. Clin. Microbiol.* **2002**, *40*, 4750–4752. [[CrossRef](#)] [[PubMed](#)]
15. Moore, D.A.J.; Mendoza, D.; Gilman, R.H.; Evans, C.A.W.; Delgado, M.G.H.; Guerra, J.; Caviedes, L.; Vargas, D.; Ticona, E.; Ortiz, J.; et al. Microscopic observation drug susceptibility assay, a rapid, reliable diagnostic test for multidrug-resistant tuberculosis suitable for use in resource-poor settings. *J. Clin. Microbiol.* **2004**, *42*, 4432–4437. [[CrossRef](#)] [[PubMed](#)]
16. Sloan, D.J.; Lewis, J.M. Management of multidrug-resistant tb: Novel treatments and their expansion to low resource settings. *Trans. R. Soc. Trop. Med. Hyg.* **2016**, *110*, 163–172. [[CrossRef](#)] [[PubMed](#)]
17. Zhang, Y.; Mitchison, D. The curious characteristics of pyrazinamide: A review. *Int. J. Tuberc. Lung Dis.* **2003**, *7*, 6–21.
18. Sengstake, S.; Bergval, I.L.; Schuitema, A.R.; de Beer, J.L.; Phelan, J.; de Zwaan, R.; Clark, T.G.; van Soolingen, D.; Anthony, R.M. Pyrazinamide resistance-conferring mutations in *pnca* and the transmission of multidrug resistant tb in georgia. *BMC Infect. Dis.* **2017**, *17*, 491. [[CrossRef](#)]
19. *Global Tuberculosis Report 2016*; World Health Organization: Geneva, Switzerland, 2016.
20. Yadon, A.N.; Maharaj, K.; Adamson, J.H.; Lai, Y.-P.; Sacchetti, J.C.; Ioerger, T.R.; Rubin, E.J.; Pym, A.S. A comprehensive characterization of *pnca* polymorphisms that confer resistance to pyrazinamide. *Nat. Commun.* **2017**, *8*, 588. [[CrossRef](#)]
21. Allana, S.; Shashkina, E.; Mathema, B.; Bablshvili, N.; Tukvadze, N.; Shah, N.S.; Kempker, R.R.; Blumberg, H.M.; Moodley, P.; Mlisana, K.; et al. *pnca* gene mutations associated with pyrazinamide resistance in drug-resistant tuberculosis, south africa and georgia. *Emerg. Infect. Dis.* **2017**, *23*, 491–495. [[CrossRef](#)]
22. Mitchison, D.A. The action of antituberculosis drugs in short-course chemotherapy. *Tubercle* **1985**, *66*, 219–225. [[CrossRef](#)]
23. Chang, K.C.; Yew, W.W.; Zhang, Y. Pyrazinamide susceptibility testing in mycobacterium tuberculosis: A systematic review with meta-analyses. *Antimicrob. Agents Chemother.* **2011**, *55*, 4499–4505. [[CrossRef](#)] [[PubMed](#)]
24. Zimic, M.; Loli, S.; Gilman, R.H.; Gutierrez, A.; Fuentes, P.; Cotrina, M.; Kirwan, D.; Sheen, P. A new approach for pyrazinamide susceptibility testing in mycobacterium tuberculosis. *Microb. Drug Resist.* **2012**, *18*, 372–375. [[CrossRef](#)] [[PubMed](#)]
25. Heifets, L.; Lindholm-Levy, P. Pyrazinamide sterilizing activity in vitro against semidormant mycobacterium tuberculosis bacterial populations. *Am. Rev. Respir. Dis.* **1992**, *145*, 1223–1225. [[CrossRef](#)] [[PubMed](#)]
26. Zhang, Y.; Wade, M.M.; Scorpio, A.; Zhang, H.; Sun, Z.H. Mode of action of pyrazinamide: Disruption of mycobacterium tuberculosis membrane transport and energetics by pyrazinoic acid. *J. Antimicrob. Chemother.* **2003**, *52*, 790–795. [[CrossRef](#)]
27. Alcántara, R.; Fuentes, P.; Antiparra, R.; Santos, M.; Gilman, R.H.; Kirwan, D.E.; Zimic, M.; Sheen, P. MODS-wayne, a Colorimetric Adaptation of the Microscopic-Observation Drug Susceptibility (MODS) Assay for Detection of *Mycobacterium tuberculosis* Pyrazinamide Resistance from Sputum Samples. *J. Clin. Microbiol.* **2019**, *57*, e01162-18. [[CrossRef](#)]
28. Wayne, L.G. Simple pyrazinamidase and urease tests for routine identification of mycobacteria. *Am. Rev. Respir. Dis.* **1974**, *109*, 147–151. [[PubMed](#)]
29. Lacroix, C.; Langlois, B.; Menager, S.; Lafont, O. Concomitant microdetermination of serum pyrazinamide and pyrazinoic acid by liquid-chromatography. *Ann. Biol. Clin.* **1987**, *45*, 297–299.

30. Lacroix, C.; Poncet, P.; Laine, G.; Guyonnaud, C.; Ray, M.; Menager, S.; Lafont, O. Microdetermination of pyrazinamide and its metabolites (2-pyrazinoic acid, 5-hydroxypyrazinoic acid, 5-hydroxypyrazinamide and pyrazinuric acid) in plasma and urine by liquid-chromatography. *J. Chromatogr. Biomed. Appl.* **1987**, *422*, 217–225. [[CrossRef](#)]
31. Shah, P.A.; Sharma, P.; Shah, J.V.; Sanyal, M.; Shrivastav, P.S. An improved lc-ms/ms method for the simultaneous determination of pyrazinamide, pyrazinoic acid and 5-hydroxy pyrazinoic acid in human plasma for a pharmacokinetic study. *J. Chromatogr. B* **2016**, *1017*, 52–61. [[CrossRef](#)]
32. Schlücker, S. Surface-enhanced raman spectroscopy: Concepts and chemical applications. *Angew. Chem. Int. Edit.* **2014**, *53*, 4756–4795. [[CrossRef](#)]
33. Jahn, I.J.; Zukovskaja, O.; Zheng, X.S.; Weber, K.; Bocklitz, T.W.; Cialla-May, D.; Popp, J. Surface-enhanced raman spectroscopy and microfluidic platforms: Challenges, solutions and potential applications. *Analyst* **2017**, *142*, 1022–1047. [[CrossRef](#)] [[PubMed](#)]
34. Bonifacio, A.; Cervo, S.; Sergo, V. Label-free surface-enhanced raman spectroscopy of biofluids: Fundamental aspects and diagnostic applications. *Anal. Bioanal. Chem.* **2015**, *407*, 8265–8277. [[CrossRef](#)] [[PubMed](#)]
35. Hidi, I.J.; Jahn, M.; Weber, K.; Bocklitz, T.; Pletz, M.W.; Cialla-May, D.; Popp, J. Lab-on-a-chip-surface enhanced raman scattering combined with the standard addition method: Toward the quantification of nitroxoline in spiked human urine samples. *Anal. Chem.* **2016**, *88*, 9173–9180. [[CrossRef](#)] [[PubMed](#)]
36. Kalkar, A.K.; Bhosekar, N.M.; Kshirsagar, S.T. Polarized raman and infrared-spectra of pyrazinamide. *Spectrochim. Acta Part A Mol. Biomol. Spectrosc.* **1989**, *45*, 635–641. [[CrossRef](#)]
37. Gunasekaran, S.; Ponnambalam, U.; Muthu, S.; Ponnusamy, S. Vibrational and normal coordinate analysis of pyrazinamide. *Asian J. Chem.* **2004**, *16*, 1513–1518.
38. Chis, V.; Pirnau, A.; Jurca, T.; Vasilescu, M.; Simon, S.; Cozar, O.; David, L. Experimental and dft study of pyrazinamide. *Chem. Phys.* **2005**, *316*, 153–163. [[CrossRef](#)]
39. Wang, Y.; Li, Y.S.; Wu, J.; Zhang, Z.X.; An, D.Q. Surface-enhanced raman spectra of some anti-tubercle bacillus drugs. *Spectrochim. Acta Part A Mol. Biomol. Spectrosc.* **2000**, *56*, 2637–2644. [[CrossRef](#)]
40. Baldwin, J.A.; Vlckova, B.; Andrews, M.P.; Butler, I.S. Surface-enhanced raman scattering of mercaptopyrindines and pyrazinamide incorporated in silver colloid adsorbate films. *Langmuir* **1997**, *13*, 3744–3751. [[CrossRef](#)]
41. Castro, J.L.; Montanez, M.A.; Otero, J.C.; Marcos, J.I. Enhanced raman-scattering from pyrazinoic acid on silver and gold sols. *Spectrosc. Lett.* **1993**, *26*, 237–244. [[CrossRef](#)]
42. März, A.; Ackermann, K.R.; Malsch, D.; Bocklitz, T.; Henkel, T.; Popp, J. Towards a quantitative sers approach—Online monitoring of analytes in a microfluidic system with isotope-edited internal standards. *J. Biophotonics* **2009**, *2*, 232–242. [[CrossRef](#)]
43. Song, H.; Tice, J.D.; Ismagilov, R.F. A microfluidic system for controlling reaction networks in time. *Angew. Chem. Int. Edit.* **2003**, *42*, 768–772. [[CrossRef](#)] [[PubMed](#)]
44. Henkel, T.; Bermig, T.; Kielpinski, M.; Grodrian, A.; Metze, J.; Köhler, J.M. Chip modules for generation and manipulation of fluid segments for micro serial flow processes. *Chem. Eng. J.* **2004**, *101*, 439–445. [[CrossRef](#)]
45. Zhang, D.M.; Xie, Y.; Deb, S.K.; Davison, V.J.; Ben-Amotz, D. Isotope edited internal standard method for quantitative surface-enhanced raman spectroscopy. *Anal. Chem.* **2005**, *77*, 3563–3569. [[CrossRef](#)] [[PubMed](#)]
46. Leopold, N.; Lendl, B. A new method for fast preparation of highly surface-enhanced raman scattering (sers) active silver colloids at room temperature by reduction of silver nitrate with hydroxylamine hydrochloride. *J. Phys. Chem. B* **2003**, *107*, 5723–5727. [[CrossRef](#)]
47. Dugandžić, V.; Hidi, I.J.; Weber, K.; Cialla-May, D.; Popp, J. In situ hydrazine reduced silver colloid synthesis—Enhancing sers reproducibility. *Anal. Chim. Acta* **2016**, *946*, 73–79. [[CrossRef](#)] [[PubMed](#)]
48. R Core Team. *R: A Language and Environment for Statistical Computing*; R Foundation for Statistical Computing: Vienna, Austria, 2014. Available online: <http://www.R-project.org> (accessed on 20 June 2019).
49. Ryan, C.G.; Clayton, E.; Griffin, W.L.; Sie, S.H.; Cousens, D.R. Snip, a statistics-sensitive background treatment for the quantitative-analysis of pixe spectra in geoscience applications. *Nucl. Instrum. Methods B* **1988**, *34*, 396–402. [[CrossRef](#)]
50. März, A.; Bocklitz, T.; Popp, J. Online-calibration for reliable and robust lab-on-a-chip surface enhanced raman spectroscopy measurement in a liquid/liquid segmented flow. *Anal. Chem.* **2011**, *83*, 8337–8340. [[CrossRef](#)]

51. Moskovits, M.; Suh, J.S. Surface selection-rules for surface-enhanced raman-spectroscopy—Calculations and application to the surface-enhanced raman-spectrum of phthalazine on silver. *J. Phys. Chem.* **1984**, *88*, 5526–5530. [[CrossRef](#)]
52. Mühlig, A.; Cialla-May, D.; Popp, J. Fundamental sers investigation of pyridine and its derivates as a function of functional groups, their substitution position, and their interaction with silver nanoparticles. *J. Phys. Chem. C* **2017**, *121*, 2323–2332. [[CrossRef](#)]
53. Arenas, J.F.; Castro, J.L.; Otero, J.C.; Marcos, J.I. Surface-enhanced raman spectra of pyrazinecarboxamide and pyrazinecarbonitrile on silver sols. *J. Raman Spectrosc.* **1992**, *23*, 249–252. [[CrossRef](#)]
54. Lee, P.C.; Meisel, D. Adsorption and surface-enhanced raman of dyes on silver and gold sols. *J. Phys. Chem.* **1982**, *86*, 3391–3395. [[CrossRef](#)]
55. Gao, R.; Choi, N.; Chang, S.-I.; Lee, E.K.; Choo, J. Real-time analysis of diaquat dibromide monohydrate in water with a sers-based integrated microdroplet sensor. *Nanoscale* **2014**, *6*, 8781–8786. [[CrossRef](#)] [[PubMed](#)]
56. Meinzen, C.; Proaño, A.; Gilman, R.H.; Caviedes, L.; Coronel, J.; Zimic, M.; Sheen, P. A quantitative adaptation of the wayne test for pyrazinamide resistance. *Tuberculosis* **2016**, *99*, 41–46. [[CrossRef](#)] [[PubMed](#)]



© 2019 by the authors. Licensee MDPI, Basel, Switzerland. This article is an open access article distributed under the terms and conditions of the Creative Commons Attribution (CC BY) license (<http://creativecommons.org/licenses/by/4.0/>).